Honda Research Institute EU
Honda Research Institute Europe GmbH
https://www.honda-ri.de/

Identification of optimal topologies for crashworthiness with the evolutionary level set method

Mariusz Bujny, Nikola Aulig, Markus Olhofer, Fabian Duddeck

2017

Preprint:

This is an accepted article published in International Journal of Crashworthiness. The final authenticated version is available online at: https://doi.org/10.1080/13588265.2017.1331493

The Version of Record of this manuscript has been published and is available in the International Journal of Crashworthiness, 02 Jun 2017, www.tandfonline.com/doi/full/10.1080/13588265.2017.1331493.

ARTICLE TEMPLATE

Identification of optimal topologies for crashworthiness with the evolutionary level set method

Mariusz Bujny[a], Nikola Aulig[b], Markus Olhofer[b] and Fabian Duddeck[a]

[a]Technical University of Munich, Arcisstraße 21, Munich, Germany; [b]Honda Research Institute Europe GmbH, Carl-Legien-Straße 30, Offenbach/Main, Germany

ARTICLE HISTORY
Compiled May 4, 2017

ABSTRACT
Structural topology optimisation methods are well established in many engineering disciplines. However, for highly non-linear problems, including crashworthiness, methods are less developed and still subject to active research. In particular, due to the simplifications made in the state-of-the-art methods as well as heuristic character of most of them, the optimality of the obtained structures is arguable. In this paper, a topology optimisation approach based on the level set method and evolutionary algorithms is presented. The method is free from the heuristic assumptions and therefore, allows for a direct optimisation of the underlying crash problem. As a result, a reliable information about the optima of crash problems can be obtained. In order to assure the consistency of the results, a comprehensive study of optimisation settings is performed and discussed. Optimisation results for 2D crash test cases are presented and general conclusions concerning the behaviour of the optimal crash structures are derived.

KEYWORDS
Crashworthiness; topology optimisation; level set method; evolutionary algorithms; optimal structures

1. Introduction

Structural topology optimisation (TO) is a research field focusing on development of methods allowing for an identification of the optimal concept structures in the early stages of the product development process. Due to the progress in the finite element method (FEM) and the growth of computational power of contemporary computers, as well as the recent advances in the manufacturing technologies, it starts to play a very important role in the industry. TO techniques are widely applied in aerospace and automotive industry, as well as in civil engineering, materials science and biomechanics. Nevertheless, in some disciplines, including crashworthiness, the use of the TO methods is very limited often due to their heuristic nature, based on assumptions that are not proven and therefore often not accepted by the engineering community. In this case, efficient gradient-based methods cannot be used directly, as a result of a highly non-linear, noisy and discontinuous character of the objective functions to be optimised, which makes analytical sensitivity information either not available or difficult to obtain. Another problem is the academic character of the state-of-the-art

CONTACT Mariusz Bujny. Email: mariusz.bujny@tum.de

methods for crash TO, indicating a need for the further research in this field. The design of crashworthiness components is an important part of the vehicle design process in the automotive industry. Target of these structures is to limit damage to vehicle and passengers in possible crash scenarios. With high demands on passive safety and increasing simulation capabilities, TO provides chances for finding the most efficient design solutions for crash requirements.

In general, state-of-the-art crash TO approaches can be divided into the following groups [19]:

- Equivalent static loads methods (ESL)
- Ground structure approaches (GSA) and permutative methods
- Bubble and graph/heuristic-based approaches
- Hybrid cellular automata techniques (HCA)
- State-based representation approaches

The ESL methods [15, 16, 20, 35] assume equivalence of static and dynamic loads and use efficient gradient-based optimisation techniques for finding optimal topologies. However, the assumption that the crash case can be replaced by a linear elastic problem is highly arguable and can be true only for selected cases, e.g. parts of the car structure that do not undergo high deformations, like the safety cell.

In GSA [21, 37], the car body structure is modelled as a system of elementary components that undergo a simplified crash behaviour. A gradient-based optimisation of the crash structure is performed based on mathematical sensitivity information that can be derived analytically for the simplified model. The main advantage of such a method is the use of non-linear crash simulations without high numerical cost. The main drawbacks of the method are the high calibration effort to achieve a realistic crash behaviour of the simplified model and the intrinsic limitation of the design space due to relatively low number of design variables and their restricted variability. The final result of an optimisation is therefore highly dependent on the ground structure that is used.

Graph and heuristic approaches [33] use rules derived from the expert knowledge to introduce topological changes, which are made in the outer optimisation loop. The inner optimisation loop deals with a common shape and size optimisation problem, which is solved with use of evolutionary optimisation methods. Although the graph and heuristic methods seem to be more reliable than the methods described above thanks to the use of explicit finite element crash simulations, the heuristic rules are not commonly accepted by the engineering community and can lead to inferior designs. The rules for topological changes are tailored for the considered problem and it is not clear how to obtain or adjust the rules for changes of the optimisation target or more complex cases.

Hybrid cellular automata techniques (HCA) [31, 36] adapt the idea of cellular automata used initially in a process model of bone remodelling. In case of crash TO, the concept of fully stressed design, well-known in linear elastic mechanics, was exploited to require a uniform energy absorption among all elements of the structure. This is not a correct assumption for thin-walled metal structures when energy absorption is maximised, due to buckling behaviour that causes local peaks in plastic deformation and hence the energy absorption is not uniform. Nevertheless, the method can be used for the cases where intrusion has to be minimised. The possibility to use non-linear FEM for crash simulations as well as fast convergence of the optimisation algorithm is an unquestionable advantage. The energy uniformity assumption also leads to optimisation of compliance for structures subject to static loads. This enables to apply

HCA for concurrent optimisation of structures subject to crash and static loads [4, 5]. Proposed recently, hybrid cellular automata for thin-walled structures (HCATWS) [19, 30, 45], extends the main concept of HCA by allowing for creation of local plastic hinge lines on the unit walls that are used instead of voxels. Still, the method has a heuristic character, which limits significantly its generality.

State-based representation approaches propose to cluster the design in a lower dimensional space of local state features, like for instance the internal energy density [6]. The material in each cluster of elements is iteratively updated based on optimising update-signal parameters by an evolutionary strategy resulting in a generic method for a gradient-based optimisation. The method was successfully applied to the problem of minimising intrusion of a structure subject to pole crash loading. Currently, however the model requires computationally expensive retraining and more application examples are required to confirm its usefulness.

Recently, an alternative crash TO approach, the evolutionary level set method (EA-LSM), being a combination of evolutionary algorithms (EA) and the level set method (LSM), was proposed [11, 13]. In LSM [18], unlike in the classical density-based approaches, the design parametrisation is not done explicitly by defining the densities of the voxels filling the design domain, but implicitly, by the level set function, which indicates the interface between the regions occupied by material and void. As a result, the material boundary can be clearly defined. It is a desirable property in the context of manufacturability and accuracy of the crash simulations, where intermediate densities present in the density-based approaches could cause severe problems. Moreover, the number of design variables can be reduced significantly by introducing geometric basis functions, which are used to define the global level set function [22]. The reduction of the number of design variables allows for application of stochastic methods for solving the optimisation problem. Those methods exhibit superior global search properties and can be used when no reliable gradient information is available, which is often the case for problems involving very complex physical phenomena, which are present in crashworthiness optimisation. Therefore, the EA-LSM can be used with great flexibility, for optimisation of problems involving different sets of objectives and constraints, without the risk of possibly incorrect simplifications that are implied by the usage of the existing heuristics. As a result, the method can identify concept designs for various optimisation criteria relying directly on evaluations of the underlying problem. Thanks to the generality of the non-gradient methods, the approach can be easily applied for optimisation of arbitrary problems in structural mechanics. Finally, the method is very promising in the context of the future industrial applications, where the high computational costs of the evolutionary algorithms[1] can be managed by means of parallelisation and reduced with use of the hybrid approaches [14].

One of the major obstacles in the development of new crash TO approaches is the lack of reliable benchmark cases and knowledge about the behaviour of the optimal crash structures. In this paper, we use the EA-LSM for identification of the best concept designs for selected crash cases. As mentioned above, without the use the heuristic assumptions in the proposed approach, the results can deliver a reliable information about the optima of the considered crash problems.

The paper is structured as follows. In Section 2 the optimisation method is de-

[1]Since the state-of-the-art methods presented above solve different optimisation problems, resulting from simplifications of the crash problem to be solved, a direct comparison of computational costs is not relevant. However, for linear elastic cases, analytical sensitivity information is available and performance of both evolutionary and gradient-based optimization algorithms can be compared for the proposed parametrisation. The comparison can be found in the paper by Bujny et al. [14].

scribed. Section 3 presents the test cases used for both validation and the actual crash optimisation. In Section 4 the validation of the method on a linear elastic problem is presented. Finally, Section 5 presents the results of numerical experiments on the selected crash problems and Section 6 summarises the paper.

2. Optimisation method

2.1. *Level set method*

Structural TO methods used today belong mostly to the group of density-based approaches. In this group, SIMP-based methods [7, 39], as well as homogenisation methods [1, 8, 29, 42] can be distinguished. In those methods, parametrisation of the design is realised by dividing the domain into a mesh of voxels that are assigned at least one continuous variable per element. By adjusting them, the optimisation algorithm changes the material distribution to obtain the optimal structural design.

The second major group of TO approaches, level set methods, are based on an implicit parametrisation of material boundaries with level set functions [2, 34, 40, 43]. In this class of methods, the interfaces between different phases of material are defined by iso-contours of a level set function Φ. As shown in Figure 1, positive values of the level set function indicate the regions occupied by material Ω, negative values define void $D\backslash\Omega$ and the boundary $\partial\Omega$ is clearly defined by the 0th iso-contour. This can be very helpful in improving accuracy of capturing mechanical response in the neighbourhood of the material boundaries and, above all, allows to avoid the intermediate material ambiguities appearing in the standard, density-based methods. Unlike in the approaches using explicit parametrisation of material interfaces (e.g. splines), introduction of topological changes (e.g. merging holes or creating connections) in LSMs is straightforward. Incorporation of such techniques as topological derivatives, in order to create new holes inside material phase, is also possible [3, 44]. Finally, most of the LSMs do not suffer from the problem of interface spatial oscillations, which depend on mesh and often appear in the density-based approaches [18].

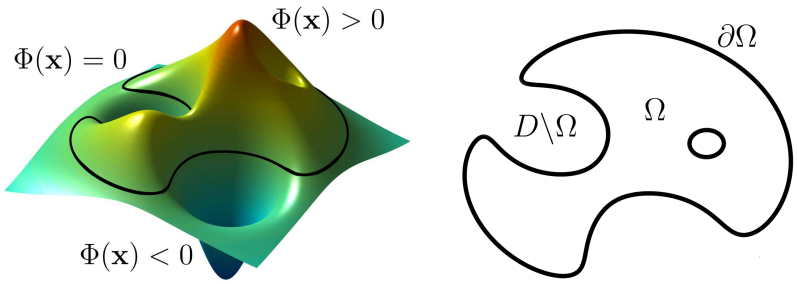

(a) An example of a level set function Φ.

(b) The material domain Ω corresponding to Figure 1(a).

Figure 1. An example of a level set function Φ and corresponding material domain Ω.

Level set TO is a relatively young discipline, but was intensively developed in the recent years. So far, it was used mainly for the problems where gradient information can be obtained analytically. Recently, the first attempts to use the method with non-gradient optimisers have been made [11, 14, 24]. Bujny et al. used LSM for the first time in crash TO [13]. In this paper, the method is used to identify the best concept structures with respect to different crash performance criteria.

2.2. *Parametrisation*

As mentioned in the introductory part of this paper, the parametrisation of the design in this work is based on the implicit level set description. The global level set function, which is mapped to the finite element mesh with use of a density-based geometry mapping [18], is composed of local basis functions of the form proposed by Guo et al. [22]. These functions can be seen as elementary beam components that can overlap and freely move within the design domain. Due to the fact that the optimal topologies in structural mechanics are usually composed of many interconnected beams (provided that the 0-1 material densities are required), this representation can describe very well a wide range of designs with a very limited number of basis functions, which is a great advantage in case of evolutionary optimisation. Below, a formal description of the method is presented.

The global level set function, Φ, is defined as follows:

$$\begin{cases} \Phi(\mathbf{x}) > 0, \mathbf{x} \in \Omega, \\ \Phi(\mathbf{x}) = 0, \mathbf{x} \in \partial\Omega, \\ \Phi(\mathbf{x}) < 0, \mathbf{x} \in D \backslash \Omega, \end{cases} \tag{1}$$

where Ω is a region, inside the design domain D, occupied by material. Consequently, $D\backslash\Omega$ refers to the part of the design domain occupied by void. $\partial\Omega$ is the interface between material and void.

Analogically, a local level set function of the ith elementary structural component is given by:

$$\begin{cases} \phi_i(\mathbf{x}) > 0, \mathbf{x} \in \Omega_i, \\ \phi_i(\mathbf{x}) = 0, \mathbf{x} \in \partial\Omega_i, \\ \phi_i(\mathbf{x}) < 0, \mathbf{x} \in D \backslash \Omega_i, \end{cases} \tag{2}$$

where Ω_i is a part of the design domain D, where the ith elementary component is located. Therefore, the part of the design occupied by the material can be defined as:

$$\Omega = \bigcup_{i=1}^{e} \Omega_i, \tag{3}$$

where e is the number of elementary components. In this work, a local level set function after Guo et al. [22] was used. For $D = \mathbb{R}^2$, $\mathbf{x} = (x, y)^T$, it can be expressed by:

$$\begin{aligned} \phi_i(\mathbf{x}) = -\Bigg(& \left(\frac{\cos\theta_i \left(x - x_{0i}\right) + \sin\theta_i \left(y - y_{0i}\right)}{l_i/2} \right)^q \\ & + \left(\frac{-\sin\theta_i \left(x - x_{0i}\right) + \cos\theta_i \left(y - y_{0i}\right)}{t_i/2} \right)^q - 1 \Bigg), \end{aligned} \tag{4}$$

where (x_0, y_0) denotes the position of the centre of a component (Figure 2(a)) of length l and thickness t. Component rotation angle is denoted by θ. As in the work by Guo et al. [22], the exponent value $q = 6$ is chosen. Figure 2(b) depicts the resulting parametrisation with the level set function defined by (4).

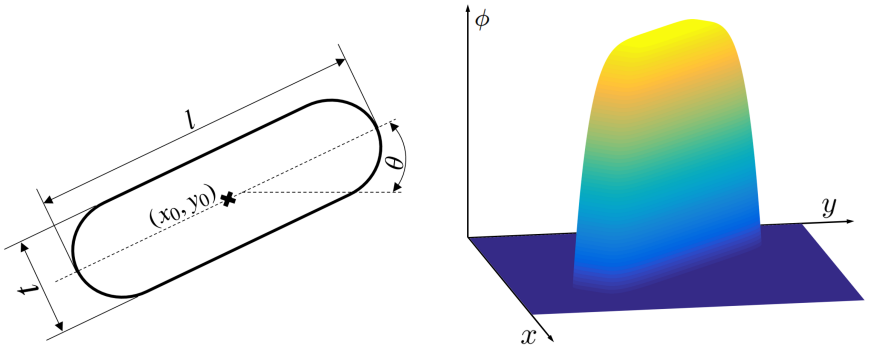

(a) Elementary structural component. (b) Level set function.

Figure 2. Elementary structural component parametrisation and the corresponding level set function (where negative values are set to zero) [13, 22].

Similarly to the other TO approaches [9], a standard density-based geometry mapping [18] is used. In this case, the relation between the global level set function and the material density[2] $\rho(\mathbf{x})$ at position $\mathbf{x} \in D$ is given by:

$$\rho(\mathbf{x}) = H(\Phi(\mathbf{x})), \tag{5}$$

where:

$$\Phi(\mathbf{x}) = \max(\phi_1(\mathbf{x}), \phi_2(\mathbf{x}), ..., \phi_m(\mathbf{x})), \tag{6}$$

and $H(x)$ denotes the Heaviside function:

$$H(x) = \begin{cases} 0, & \text{if } x < 0 \\ 1, & \text{if } x \geq 0. \end{cases} \tag{7}$$

In Figure 3, an exemplary layout of structural components for the compliance minimisation of the standard cantilever beam benchmark case is presented.

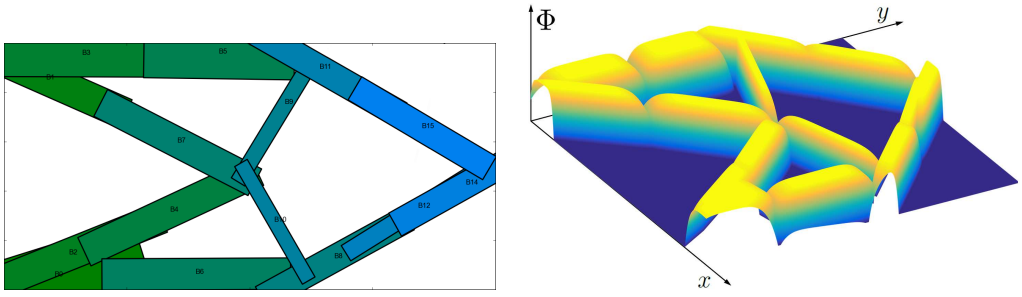

(a) Layout of structural components. (b) Corresponding level set function.

Figure 3. Exemplary layout of structural components for the compliance minimisation for the cantilever beam problem [9, 13].

[2]In the FE discretisation, $\rho(\mathbf{x}) = 0$ is equivalent to a deletion of the finite element from the mesh.

2.3. *Optimisation problem*

In this paper, the following form of optimisation problems is assumed:

$$\begin{aligned} &\min_{\mathbf{z}} f_{obj}(\mathbf{z}),\ \mathbf{z} \in \mathbb{R}^n; \\ &\text{s.t. } \mathbf{r}(t) = \mathbf{0}; \\ &\quad g_j(\mathbf{z}) \leq 0,\ j = 1, ..., p, \end{aligned} \tag{8}$$

where f_{obj} denotes the objective function to be minimised and g_j are the inequality constraints. Vector $\mathbf{z}$ is the vector of design variables, collecting all parameters defining e basis functions, and $\mathbf{r}(t) = \mathbf{0}$ relates to the dynamic equilibrium at time t.

In Section 4, compliance C is considered as the objective function f_{obj} and $g_1(\mathbf{z}) = V(\mathbf{z}) - V_{req} \leq 0$ is the only constraint, requiring the volume of the structure V to be lower than or equal to V_{req}, being 50% of the design domain volume. In Section 5.1, pole intrusion d is the minimised objective, while $g_1(\mathbf{z}) = m(\mathbf{z}) - m_{req} \leq 0$ is a constraint on the mass of the structure m, where m_{req} corresponds to 50% of the mass of the design domain filled entirely with material. Finally, Section 5.2 deals with the problem of mass m minimisation with a constraint on the intrusion of the impactor d: $g_1(\mathbf{z}) = d(\mathbf{z}) - d_{max} \leq 0$ and a constraint on its maximal acceleration a: $g_2(\mathbf{z}) = a(\mathbf{z}) - a_{max} \leq 0$. Formulation (4) with $q = 6$ accounts for negative values of the parameters, so no additional constraints to prohibit it are necessary.

Application of evolutionary algorithms to the constrained optimisation task given by the Equation (8) is possible after a transformation of the fitness function according to the exterior penalty method [17, 38]:

$$f(\mathbf{z}) = f_{obj}(\mathbf{z}) + c \sum_{j=1}^{p} \max\left(0, g_j(\mathbf{z})\right), \tag{9}$$

where c denotes a weighting constant that penalises the infeasible designs.

2.4. *Optimisation algorithm*

For solving non-linear optimisation problems, considered in this paper, the state-of-the-art covariance matrix adaptation evolution strategy (CMA-ES) [27] is used. CMA-ES is a derandomised evolutionary strategy, which, based on the previous successful search steps, applies an adaptation of the covariance matrix of the normal probability distribution used in the mutation operator [25]. This is to some extent similar to the gradient-based quasi-Newton methods, where the inverse of the Hessian matrix is iteratively estimated with the progress of the optimisation process. Particularly, CMA-ES is very effective in minimizing unimodal functions [25], but the superiority of the method on non-separable and ill-conditioned problems has been also shown [27]. The method was further extended by the rank-μ-update [28, 32] to allow for a more effective use of the information from large populations without deteriorating the performance when small populations are considered. In this work, the Python implementation [26] of this method was used.

3. Test cases

In the following section, a description of the test cases used for initial validation of the proposed method, as well as the actual optimisation of crash cases, is presented.

3.1. *Linear elastic cases*

The initial validation of the EA-LSM is done on the standard cantilever beam problem and the results are compared with the ones presented in the literature [9]. Beside the aspect ratio of the design domain of 1:2, presented in Figure 4(a), optimisations for 1:1 and 1:3 aspect ratios are realised.

The further validation is carried out on a test case corresponding directly to the crash case that is considered in this paper. As in the crash case, a topology of a rectangular beam fixed on both ends is optimised. A unit load is applied on the upper edge of the beam, exactly at the point, where the contact with the impactor takes place.

For both cases, material having properties as specified in Table 1 is used.

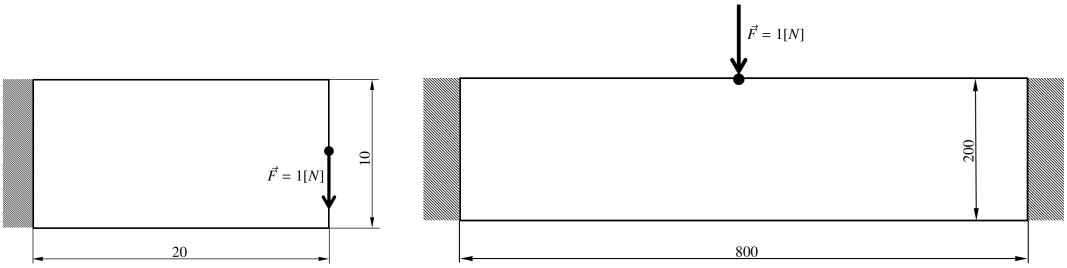

(a) Cantilever beam. (b) Transverse bending.

Figure 4. Design domain, initial and boundary conditions for the static cases used for validation of the EA-LSM. Dimensioning in [mm].

Table 1. Configuration of the static test cases used for validation.

Property	**Symbol**	**Value**	**Unit**
Young's modulus	E	$2.1 \cdot 10^5$	MPa
Poisson's ratio	ν	0.3	-
Load	F	1	N
Required volume fraction	V_f	50%	-
Mesh resolution for cantilever beam	-	100 x 50	-
Mesh resolution for transverse bending	-	160 x 40	-
Solver	-	CalculiX 2.9	-
Element type	-	Four-node shell element	-

3.2. *Non-linear crash cases*

All crash experiments are carried out for the same geometry of the design domain. As mentioned before, a rectangular beam fixed at both ends and impacted in the middle

by a cylindrical pole is considered (Figure 5). Impactor mass and velocity are varied from the reference value in different experiments.

In order to keep the generality of the results by preserving simplicity, for all crash cases, an elastic-plastic material model with linear hardening was used. Neither strain-rate dependency of the mechanical properties nor failure modelling were taken into account. The properties of the material are presented in Table 2.

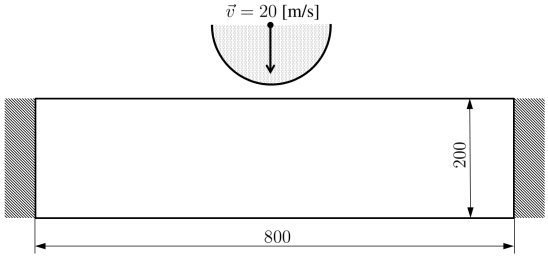

Figure 5. Design domain, initial and boundary conditions for the investigated crash case. Dimensioning in [mm].

Table 2. Configuration of the crash test case.

Property	**Symbol**	**Value**	**Unit**
Material model	-	Piecewise linear plasticity	-
Material density	ρ	$2.7 \cdot 10^3$	kg/m^3
Young's modulus	E	$7.0 \cdot 10^4$	MPa
Poisson's ratio	ν	0.33	-
Yield strength	R_e	241.0	MPa
Tangent modulus	E_{tan}	70.0	MPa
Static coefficient of friction	μ_s	0.2	-
Dynamic coefficient of friction	μ_s	0.2	-
Material model of the pole	-	Rigid	-
Reference pole velocity	v	20	m/s
Reference pole mass	m_p	11.815	kg
Pole diameter	D	139.154	mm
Required structure mass	m_{req}	2.16	kg
Mesh resolution	-	80 x 20	-
Solver	-	LS-DYNA R7.1.1	-
Element formulation	ELFORM	Constant stress solid element	-
Hourglass control	IHQ	Flanagan-Belytschko	-
Contact model	-	Penalty method	-

4. Validation for linear elastic cases

In this section, a comprehensive parameter sensitivity study of the proposed method is presented. Due to the high computational costs of the crash simulations and because of no clearly defined reference solutions for the crash load cases, a validation of the proposed method on a linear elastic problem is carried out.

4.1. *Cantilever beam*

In order to evaluate the correctness of the proposed method, the standard cantilever beam benchmark case [9] is considered. Boundary conditions and the design domain are depicted in Figure 4(a). A diagonal initial layout of the level set basis functions, as shown in Figure 7, is used. A comparison of best topologies obtained within 30 optimisation runs of the proposed method with the topologies optimised with the SIMP approach are presented in Table 3.

Table 3. Comparison of the topologies obtained with the evolutionary level set method (EA-LSM) and based on the state-of-the-art solid isotropic material with penalisation approach (SIMP) [9] for 50% volume fraction.

	Optimised topology	
Aspect ratio	EA-LSM	SIMP
1:1		
1:2		
1:3		

The results obtained with the proposed method are consistent with the SIMP approach. With only 16 level set basis functions, the method is able to develop structures of high complexity, as in the case of the 1:3 aspect ratio. However, the discrepancy between the EA-LSM and SIMP designs grows with rising complexity of the structures, reflecting the limiting effect of restricting the number of basis functions.

4.2. *Transverse bending*

The further investigations regarding the parameter sensitivity study were carried out based on the optimisation problem illustrated in Figure 4(b). This test case corresponds directly to the crash scenarios considered in the next sections, and therefore, allows for formulation of conclusions that, most probably, hold also for the crash test cases. In Figure 6, a comparison of designs obtained with the EA-LSM and SIMP approaches is presented. Again, the designs exhibit very strong similarities, proving the validity of the proposed method.

4.3. *Choice of the initial design*

The choice of the initial positions of the level set basis functions in the proposed method has to be defined in the initial setup. It can be demonstrated that unfavourable

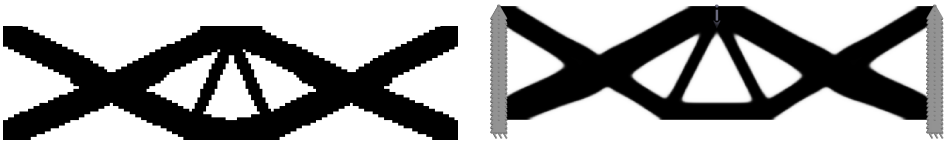

(a) EA-LSM. (b) SIMP.

Figure 6. Comparison of the topologies optimised with the EA-LSM (the best design out of 30 obtained in independent optimisation trials) and based on the SIMP approach [9, 41]. Both designs were obtained for 50% volume fraction constraint.

initialisations might lead to convergence of the algorithm to a local optimum or even failure of the optimisation process. Hence, an initial design that shows generally good performance over a wide range of optimisation problems should be chosen. A good optimisation method should exhibit also relative invariance with respect to the choice of the initial design. The strong dependency of the final design with respect to the choice of the initial ground structure is one of the main criticisms of the ground structure approaches and limits significantly their practical use. Here, we analyse the influence of the initial layout of basis functions on the convergence properties of the proposed approach.

In this section, an assessment of the proposed method with respect to the initial layout of the level set basis functions is presented. Three different layouts of the level set basis functions are considered - diagonal, orthogonal, and a filled one, resulting in material occupying the entire design domain, as shown in Figure 7.

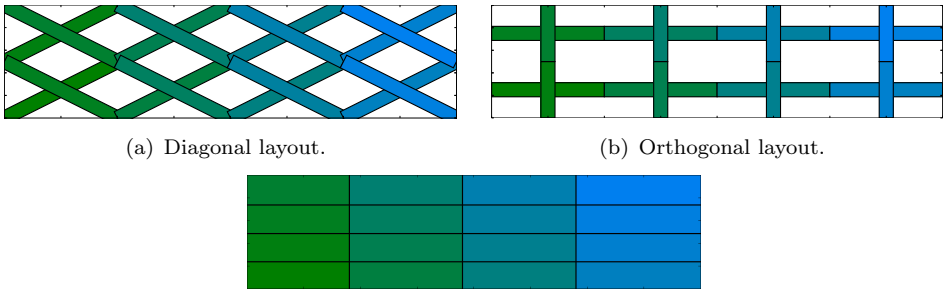

(a) Diagonal layout. (b) Orthogonal layout.

(c) Filled layout.

Figure 7. Schematic illustration of the three tested initial layouts of the level set basis functions.

To evaluate the impact of the initial design on the final, optimised topologies, for each layout, 30 optimisation runs were carried out. The results are visualised in the box plot shown in Figure 8.

From the mechanical point of view, the initial design corresponding to the diagonal layout of level set basis functions, is almost 9 times stiffer than that of the orthogonal layout, being a much better starting point for the optimisation. On the other hand, the design initialised with the filled layout violates strongly the volume constraint, leading to very high values of the penalty, which contributes to the fitness function (Equation (9)). As a result, the optimisations initialised with the orthogonal and the filled layouts much more frequently lead to local optima, as shown in Table 4. This explains why on average, the performance of the designs generated from the diagonal layout is higher[3]. Nevertheless, for all initial layouts, the same types of topologies can be obtained, which has been illustrated in Figures 9, 10 and 11. This shows that, as long

[3]This was validated with the Wilcoxon rank sum test. The null hypothesis of equal medians was rejected at the 1% significance level.

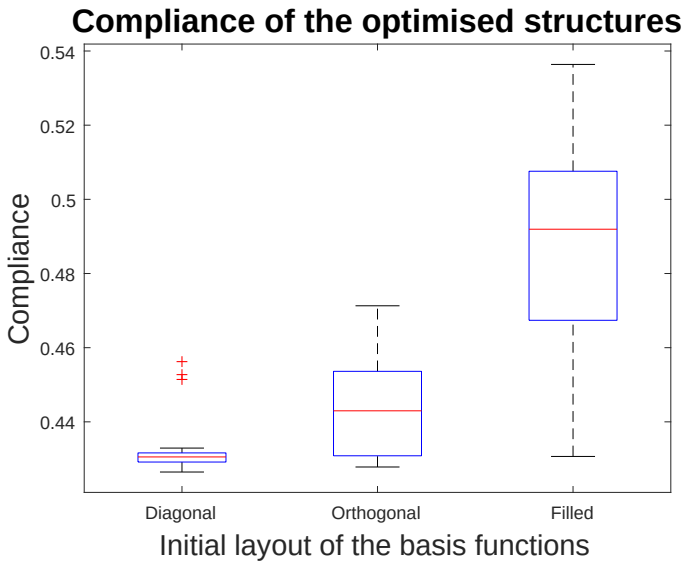

Figure 8. Box plot for 30 optimisation runs of the ESLM for the compliance minimisation problem for three different initial layouts of the level set basis functions. Compliance normalised with the initial value. On each box, the central red line indicates the median, and the bottom and top edges of the blue box indicate the 25th (q_1) and 75th (q_3) percentiles of the normalised compliance values from the 30 runs. The whiskers (dash black lines) extend to the most extreme data points not considering outliers, and the outliers are plotted individually using the red '+' symbol. Points are considered outliers, if they are greater than $q_3 + 1.5\,(q_3 - q_1)$ or less than $q_1 - 1.5\,(q_3 - q_1)$.

Table 4. Two main topology types obtained with the proposed method and the frequency with which they have been developed in 30 optimisation runs for three different types of the initial layout of the level set basis functions. Compliance normalised with the initial value.

Topology type[a]	Compliance	Probability of a given topology		
		Diagonal layout	Orthogonal layout	Filled layout
	0.4276	90%	47%	3%
	0.4527	10%	27%	7%

[a]The identification of topology types by visual inspection is not always an easy task and is very subjective. Therefore, in order to avoid errors related to a different interpretation of results, only the designs strictly consistent with the presented ones have been counted and the others were ignored.

as the choice of the initial design is not particularly unfavourable (e.g. when all basis functions are gathered in a small part of the design domain), the global optimum of the optimisation problem can be found provided that the number of trials is sufficiently high. This justifies the choice of just a one initial layout of basis functions for the further investigations regarding the optimal structures for different crash problems. Since the diagonal layout is the most frequently used in the literature [22] and exhibits good performance for the selected test cases, it will be a base for the investigations for different crash problems in this paper.

All in all, although our method exhibits some similarities to the ground structure

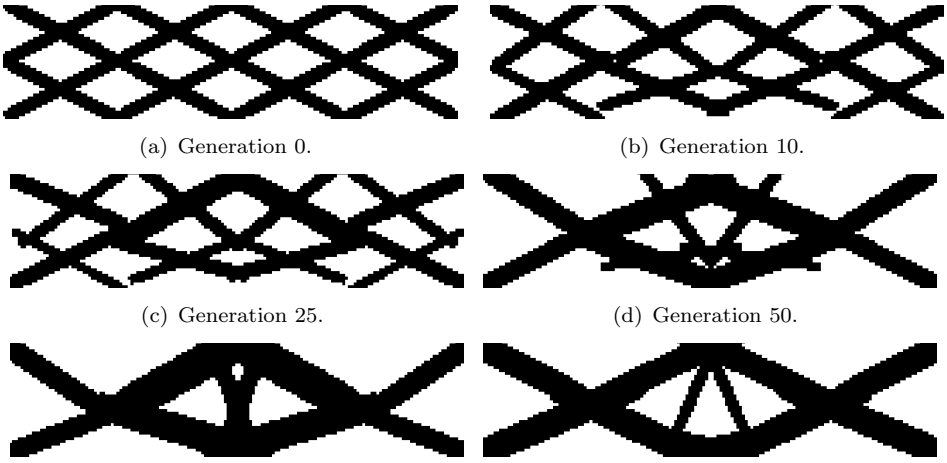

(a) Generation 0. (b) Generation 10.

(c) Generation 25. (d) Generation 50.

(e) Generation 100. (f) Generation 927.

Figure 9. Evolution of the best design through the optimisation process for the diagonal initial layout of the level set basis functions.

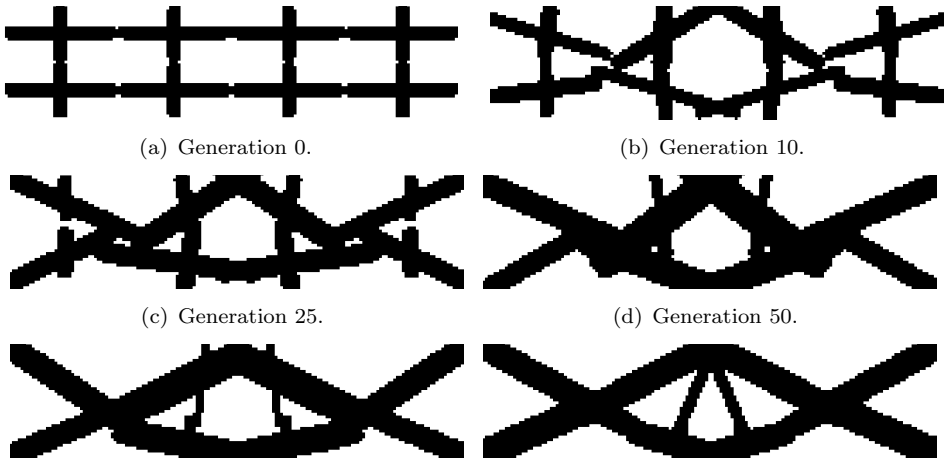

(a) Generation 0. (b) Generation 10.

(c) Generation 25. (d) Generation 50.

(e) Generation 100. (f) Generation 874.

Figure 10. Evolution of the best design through the optimisation process for the orthogonal initial layout of the level set basis functions.

approaches, thanks to relatively high design flexibility allowing basis functions to move inside the design domain, and the good global search properties of evolutionary algorithms, the quality of the obtained results does not depend very strongly on the initial positioning of the level set basis functions.

4.4. *Effect of the mesh size*

Mesh-dependency is one of the main problems in the density-based approaches (e.g. SIMP [9]) and requires additional techniques like perimeter control, density or sensitivity filtering [9]. This is caused by the direct coupling of the parametrisation of the optimisation problem with the finite element mesh. However, in the EA-LSM, where the design is parameterised by the level set function, this problem does not appear. To show this, 30 optimisation runs for 3 different finite element mesh sizes have been carried out. The best designs are shown in Figure 12.

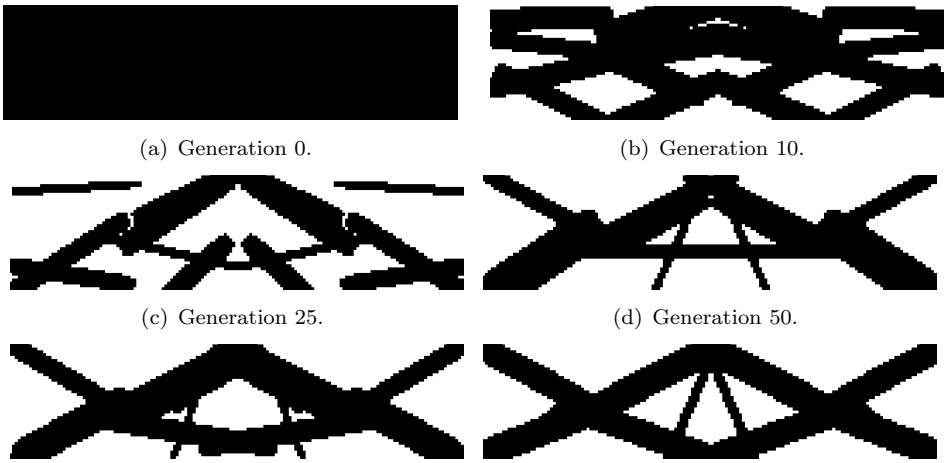

(a) Generation 0. (b) Generation 10.

(c) Generation 25. (d) Generation 50.

(e) Generation 100. (f) Generation 1000.

Figure 11. Evolution of the best design through the optimisation process for the filled initial layout of the level set basis functions.



(a) Mesh size: 80 x 20. (b) Mesh size: 160 x 40. (c) Mesh size: 320 x 80.

Figure 12. The best designs obtained in 30 optimisation runs with 3 different FE mesh sizes.

The final designs exhibit very good invariance with respect to the mesh size. Finer meshes result in better finite element modelling and not in more detailed structures, which is a desired behaviour of a TO method [9].

Unlike in the state-of-the-art methods, due to the macroscopic parametrisation type, the checkerboard problem [9] does not appear in the proposed approach. This might happen for a very high number of basis functions provided that the mesh resolution is kept on a low level, making the parametrisation to some extent similar to the density-based approaches. Nevertheless, this is of a limited practical interest, since the convergence velocity of the proposed method decreases strongly as the number of design variables is increased. Therefore, it makes no sense to increase the number of basis functions while keeping the resolution of the finite element mesh on a low level to reduce the computational costs.

4.5. *Influence of the number of basis functions*

It is well-known that for TO, when 0-1 material density is required, there are no solutions of the optimisation problem in its continuous formulation [9]. It is no longer the case for the discretised version of the same problem, but it results in gradual improvement of performance with rising complexity of the structure. However, in engineering applications, it is often recommended to keep the complexity on a relatively low level.

In the ESLM, the complexity of the structure can be controlled explicitly with the number of level set basis functions and the minimal thickness of the corresponding beam components. In the following section, the influence of the number of basis functions on the optimisation results is investigated.

In order to evaluate it, an initial design consisting of 64 level set basis functions, resulting from doubling the initial resolution of basis functions in vertical and hori-

zontal direction, is considered. Figure 13 shows the initial design and the best design obtained within 30 optimisation runs.

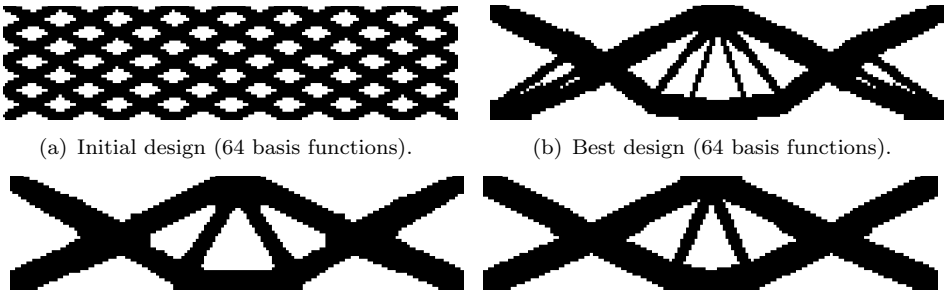

(a) Initial design (64 basis functions).

(b) Best design (64 basis functions).

(c) Optimised design (64 basis functions) closest to the best design for 16 basis functions.

(d) Best design (16 basis functions).

Figure 13. Designs obtained in 30 optimisation runs with 64 and 16 level set basis functions.

As expected, extension of the search space by introducing more basis functions, led to development of a more complex structure, exhibiting better performance than the one obtained for 16 basis functions (ca. 1.65% reduction of compliance). Nevertheless, even for a parametrisation with 64 basis functions, a topology very close to the best design obtained for 16 basis functions can be developed (Figure 13). This time, however, it corresponds just to a local optimum in the extended design space. In principle, development of topologies of different complexity for a selected number of basis functions could be also regulated through an appropriate perimeter penalisation (which might be also used to prohibit creation of low complexity structures), similar to the perimeter control in the density-based methods [9]. However, from the point of view of computational costs, it is much more efficient to limit the number of basis functions used for the parametrisation of the level set function.

In this research, the main focus is to derive some general conclusions about the optimal topologies for selected crash problems. Therefore, low complexity is not only necessary in the context of limited computational resources, but also from the perspective of preserving generality and practical relevance of the obtained results.

Taking into account the conclusions formulated above, we accept 16 level set basis functions as sufficient to represent a wide range of different topologies of acceptable complexity. Second parameter regulating the complexity, the beam thickness threshold (below which components are removed from the structure), is kept on a level corresponding to the size of a single finite element, i.e. 20 [mm].

5. Experiments for non-linear crash cases

The experiments conducted for the crash test case are structured into two sections. The two sections consider different objective functions that capture typical requirements in the crashworthiness domain. Primarily, in the first section, we analyse also effects of different loadings and the influence of the mesh resolution.

5.1. *Intrusion minimisation with mass constraint*

In case of such vehicle components as pillars, rockers or door reinforcements, it is crucial to limit the intrusion of the impactor to the safety cell. As a result, in the following section, the intrusion minimisation problem with mass constraint is considered.

5.1.1. Effect of impact velocity for constant impactor mass

In order to assess the influence of varying impact velocity (impact energy) on the optimisation results, 30 optimisation trials for 3 velocity levels were carried out. For each case, at least 3 groups of different topology types, most probably corresponding to different (local) optima, can be distinguished. Those results are presented in Table 5, where each group is represented by 3 best designs of a given class obtained in the 30 runs of the optimisation algorithm. The best designs derived for each impact velocity are summarised in Table 6.

Table 5. Comparison of the best designs for the intrusion minimisation problem with different impact velocities and constant mass of the impactor.

	Designs in groups representing different (local) optima		
Velocity	Best optimum	Second best optimum	Third best optimum
10 [m/s]	Lowest intrusion: 5.18 [mm] 	Lowest intrusion: 5.22 [mm] 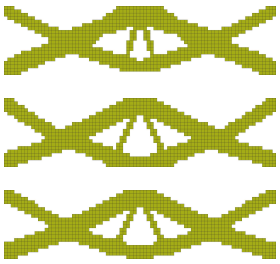	Lowest intrusion: 5.24 [mm] 
20 [m/s]	Lowest intrusion: 15.01 [mm] 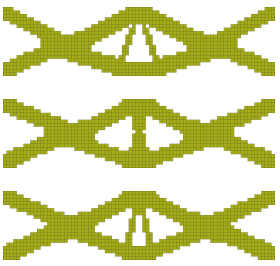	Lowest intrusion: 15.22 [mm] 	Lowest intrusion: 15.37 [mm] 
40 [m/s]	Lowest intrusion: 51.30 [mm] 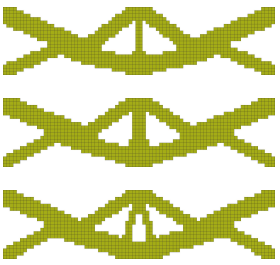	Lowest intrusion: 51.79 [mm] 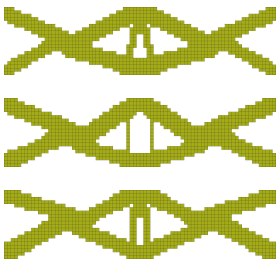	Lowest intrusion: 53.76 [mm] 

From the results presented above it can be concluded that with the rising impact velocity, the optimal topology changes gradually from the 'supporting' structure, were the members in compression play the most important role, to the 'hanging' structure, which reacts mainly through tensioning the beams that are the most distant from

Table 6. Comparison of the best designs for constant impactor mass. Percentage values express growth of intrusion with respect to the design optimised for a given impact velocity.

Design	Optimised for	Intrusion at different velocities		
		10 [m/s]	20 [m/s]	40 [m/s]
	10 [m/s]	5.18 [mm]	15.09 [mm] +0.51%	53.48 [mm] +4.25%
	20 [m/s]	5.18 [mm] +0.06%	15.01 [mm]	52.64 [mm] +2.62%
	40 [m/s]	5.27 [mm] +1.70%	15.21 [mm] +1.32%	51.30 [mm]

the impactor. Similar results were presented by Buhl et al. [10], where the topologies obtained for linear and non-linear modelling (corresponding to some extent to the crash cases considered here) were compared. To ensure that this tendency really holds and a development of different structures for different impact velocities is not a result of finding only a local optimum, performance of each design is evaluated for 3 different velocities (Table 6). This proves that each of those designs is only the best for the velocity that it has been optimised for and truly outperforms the best designs obtained for different impact velocities. It is interesting to note that the design obtained for the highest impact velocity is also the most robust one, exhibiting relatively good performance for every impact velocity (growth of intrusion with respect to the design optimised for a given impact velocity always lower than 2%). Moreover, Table 5 shows that for each impact velocity, usually similar designs (corresponding the local optima) are found, but their relative quality changes with velocity. For instance, the group of the best designs obtained for impact velocity of 10 [m/s] corresponds to the second best group of the designs optimised for 20 [m/s]. Similarly, the second best group for 10 [m/s] impact velocity corresponds to the best design obtained for 20 [m/s]. It seems that the global optimum for 10 [m/s] became a local optimum for 20 [m/s], and vice versa, the global optimum for 20 [m/s] is a local optimum for 10 [m/s]. Similar relationships can be found also for the other groups of designs in Table 5. Interestingly, not only the best design obtained for the impact velocity of 20 [m/s], but also the third group for every velocity exhibits some similarities to the optima obtained in the optimisations for the static case (Table 4). This justifies to some extent the use of the ESL for the intrusion minimisation problem and shows that the other optima for the static case might be also interesting in the context of crash TO.

In order to understand better the results, we concentrate on evaluation of the best designs only. Figure 14 shows the evolution of the impactor's intrusion over time. Corresponding deformations and stresses during the loading phase are depicted in Figures 16, 18 and 20. Effective plastic strain distributions are shown in Figures 15, 17 and 19. Force-displacement curves for the best designs are presented in Figure 21 and energy balance for those designs is shown in Figure 22.

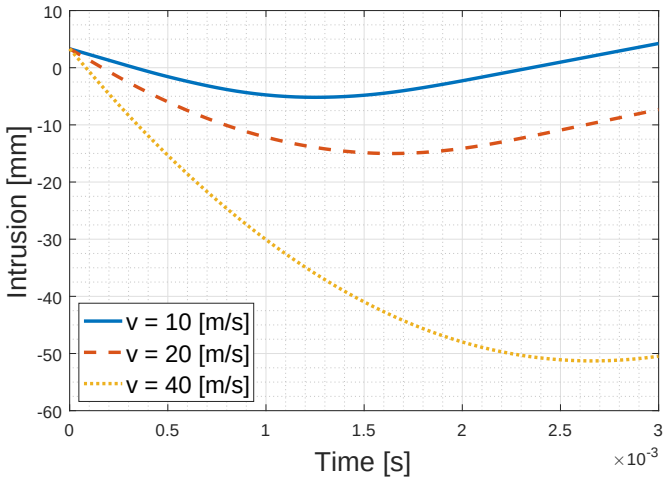

Figure 14. Intrusions for the best designs for constant impactor mass in dependency of the velocity.

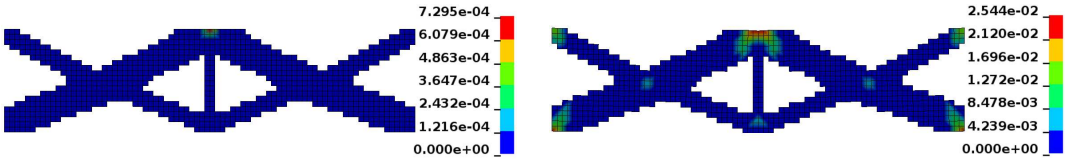

(a) After 0.3 ms, start of plastic reactions. (b) After 1.25 ms, time of maximal intrusion.

Figure 15. Effective plastic strain distribution for the best design optimised for 10 m/s impact velocity, for constant impactor mass.

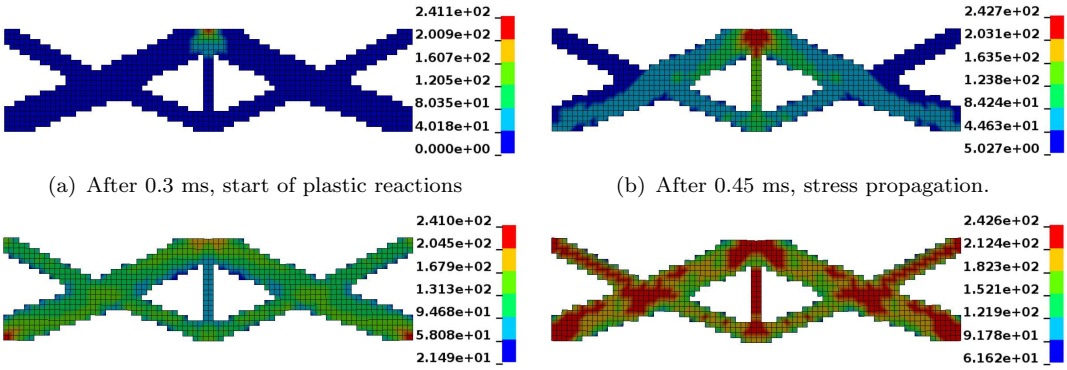

(a) After 0.3 ms, start of plastic reactions (b) After 0.45 ms, stress propagation.

(c) After 0.55 ms, stress propagation. (d) After 1.25 ms, time of maximal intrusion.

Figure 16. Von Mises stress distribution (in [MPa]) during the crash for the best design optimised for the impact velocity of 10 [m/s], for constant impactor mass.

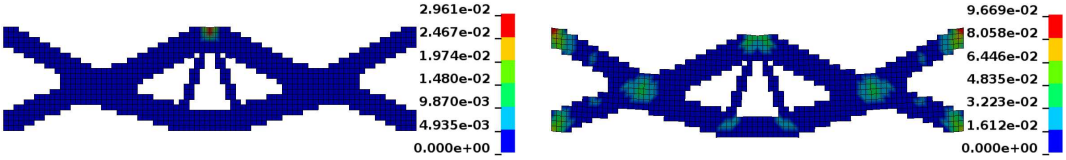

(a) After 0.2 ms, start of plastic reactions. (b) After 1.65 ms, time of maximal intrusion.

Figure 17. Effective plastic strain distribution for the best design optimised for 20 m/s impact velocity, for constant impactor mass.

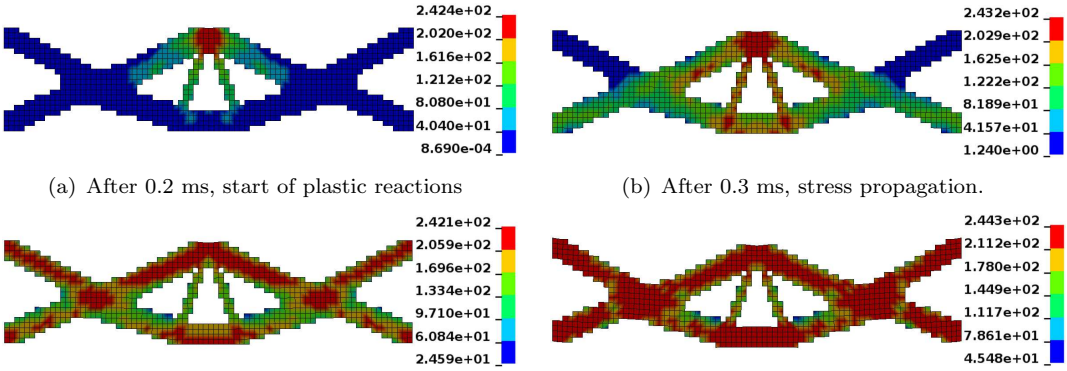

(a) After 0.2 ms, start of plastic reactions

(b) After 0.3 ms, stress propagation.

(c) After 0.4 ms, stress propagation.

(d) After 1.65 ms, time of maximal intrusion.

Figure 18. Von Mises stress distribution (in [MPa]) during the crash for the best design optimised for the impact velocity of 20 [m/s], for constant impactor mass.

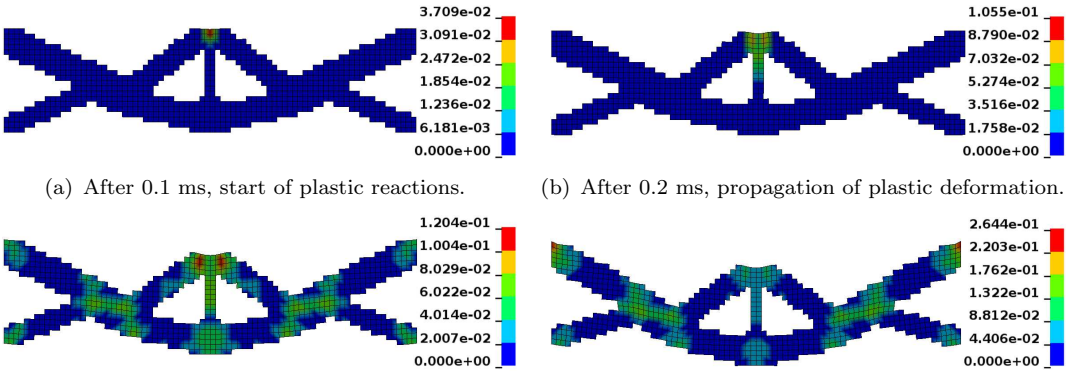

(a) After 0.1 ms, start of plastic reactions.

(b) After 0.2 ms, propagation of plastic deformation.

(c) After 1 ms, propagation of plastic deformation.

(d) After 2.65 ms, time of maximal intrusion.

Figure 19. Effective plastic strain distribution for the best design optimised for 40 m/s impact velocity, for constant impactor mass.

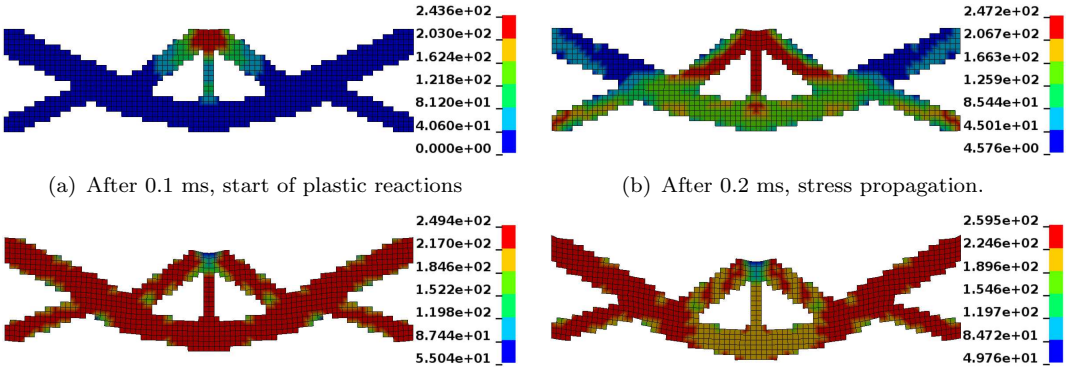

(a) After 0.1 ms, start of plastic reactions

(b) After 0.2 ms, stress propagation.

(c) After 1 ms, stress propagation.

(d) After 2.65 ms, time of maximal intrusion.

Figure 20. Von Mises stress distribution (in [MPa]) during the crash for the best design optimised for the impact velocity of 40 [m/s], for constant impactor mass.

As shown in Figures 15 and 16, the structure optimised for the impact velocity of 10 [m/s] reacts mostly elastically, yielding mainly in the regions either being in contact with the impactor or close to the supports. Therefore, it is interesting that this structure differs significantly from the one obtained for the corresponding static case (Figure 6), which shows the importance of the inertial effects even for the cases

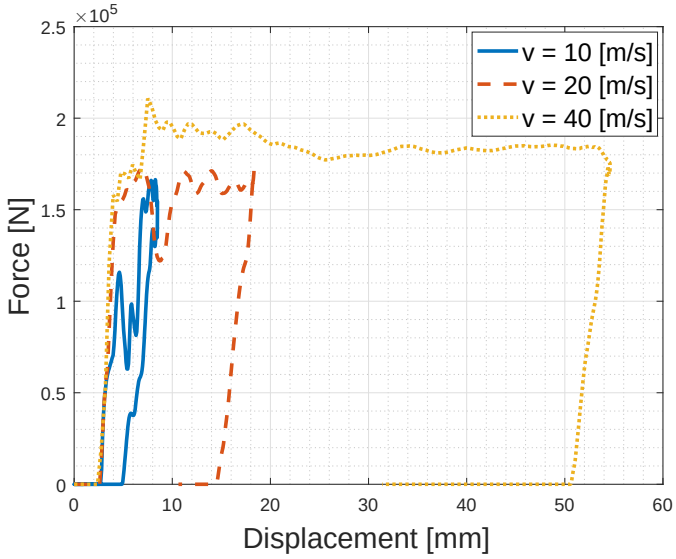

Figure 21. Force-displacement curves for the best designs for constant impactor mass, optimised for different impact velocities.

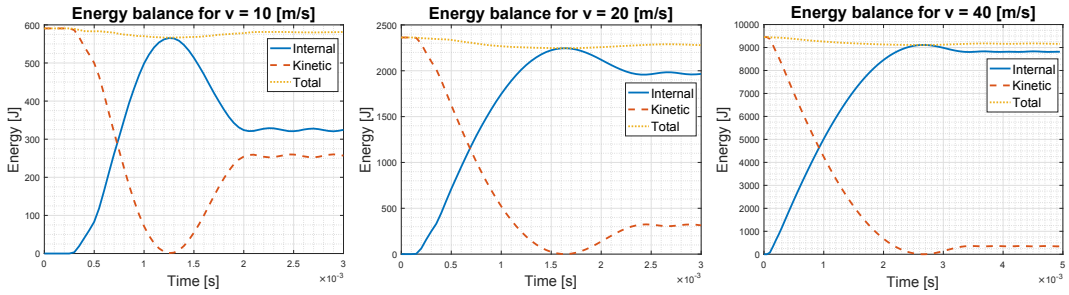

Figure 22. Energy balance for the best designs for constant impactor mass, optimised for different impact velocities.

involving very low deformations.

With rising impact velocity, a gradual change from a continuous progress of plastification of the structure in time to a two-phase plastification for the highest impact velocity can be observed (Figure 19). First, the plastification of the beams close the impactor takes place and the members in the bottom corners of the design domain are strongly compressed. In the second phase of the impact, the main, 'hanging' beam absorbs energy via tensioning and the beams in the bottom corners are strongly bended.

It should be noted, that for all of the cases presented in this section, buckling behaviour is avoided. To achieve that for cases involving strong deformations, the importance of the parts of the structure working in tension grows.

An interesting aspect is a very good homogeneity of stress distribution during the loading phase for all impact velocities. On the other hand, this is not the case for the internal energy, concentrated mainly in the regions of the highest effective plastic strains, which seems to be interesting in the context of heuristic criterion used in the HCA methods, assuming uniform energy absorption by the optimal structure. Apparently, for the intrusion minimisation case, a criterion closer to the idea of fully stressed design should be taken into account.

5.1.2. Effect of impact velocity for constant impact energy

In order to investigate the influence of inertial effects on the optimised topologies, another 2 test cases were introduced. This time, the impact energy was kept on a constant level through an appropriate scaling of the mass of the impactor for different impact velocities. The impact for velocity of 20 [m/s] served as the reference case. The best designs obtained for different impact velocities are presented in Table 7.

Table 7. Comparison of the best designs for constant impact energy. Percentage values express growth of intrusion with respect to the design optimised for a given impact velocity.

Design	Optimised for	Intrusion at different velocities		
		10 [m/s]	20 [m/s]	40 [m/s]
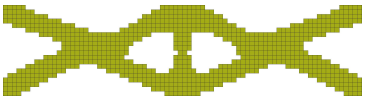	10 [m/s]	15.15 [mm]	15.04 [mm] +0.17%	14.69 [mm] +2.16%
	20 [m/s]	15.15 [mm] +0.01%	15.01 [mm]	14.57 [mm] +1.38%
	40 [m/s]	15.54 [mm] +2.57%	15.38 [mm] +2.48%	14.38 [mm]

The results show that the inertial effects have significant impact on the type of topology that is formed during the optimisation process. This is interesting since it questions the use of the ESL method when high deformations are involved.

This time, the supporting structure was the best for the highest impact velocity. This is understandable, since this case corresponds to the lowest momentum of the impactor and involves relatively small plastic deformations, which makes this problem similar to the one for low impact velocity when the mass of the impactor is kept constant. In addition, this design is the least robust with respect to different impact velocities when energy is kept constant (intrusion growth with respect to the reference case always above 2%).

Deformed structures and the corresponding effective stress distributions are depicted in Figures 24 and 26. Effective plastic strain distributions are shown in Figures 23 and 25. Force-time and force-displacement curves for the best designs are presented in Figure 27 and energy balance for those designs is shown in Figure 28.

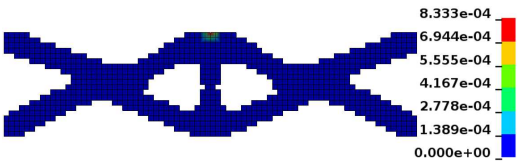

(a) After 0.3 ms, start of plastic reactions.

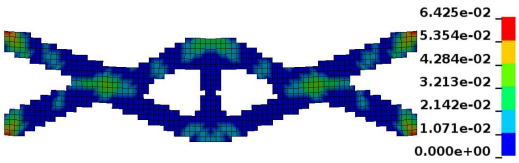

(b) After 3.2 ms, time of maximal intrusion.

Figure 23. Effective plastic strain distribution for the best design optimised for 10 m/s impact velocity, for constant impact energy.

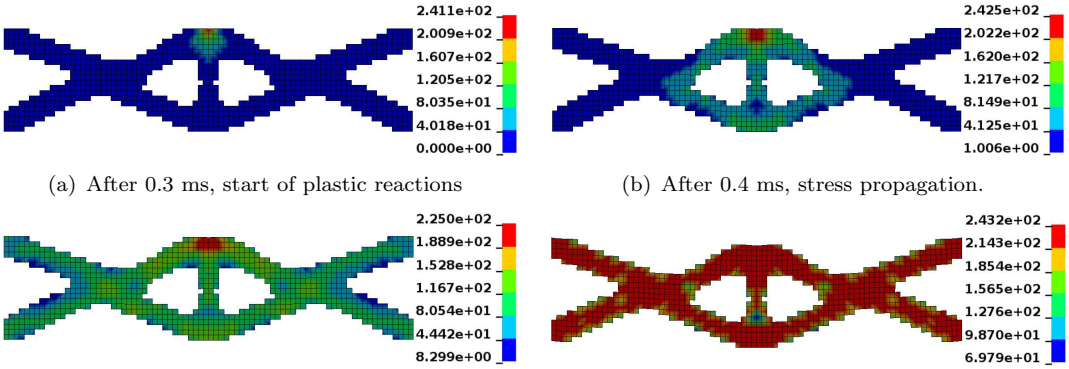

(a) After 0.3 ms, start of plastic reactions

(b) After 0.4 ms, stress propagation.

(c) After 0.5 ms, stress propagation.

(d) After 3.2 ms, time of maximal intrusion.

Figure 24. Von Mises stress distribution (in [MPa]) during the crash for the best design optimised for the impact velocity of 10 [m/s], for constant impact energy.

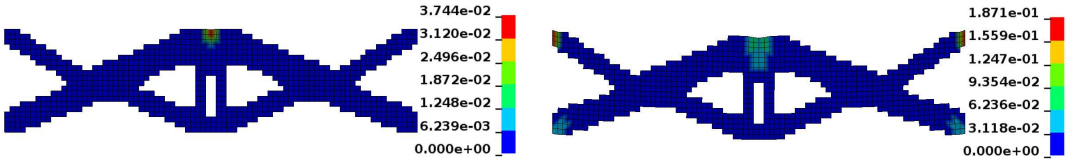

(a) After 0.1 ms, start of plastic reactions.

(b) After 0.9 ms, time of maximal intrusion.

Figure 25. Effective plastic strain distribution for the best design optimised for 40 m/s impact velocity, for constant impact energy.

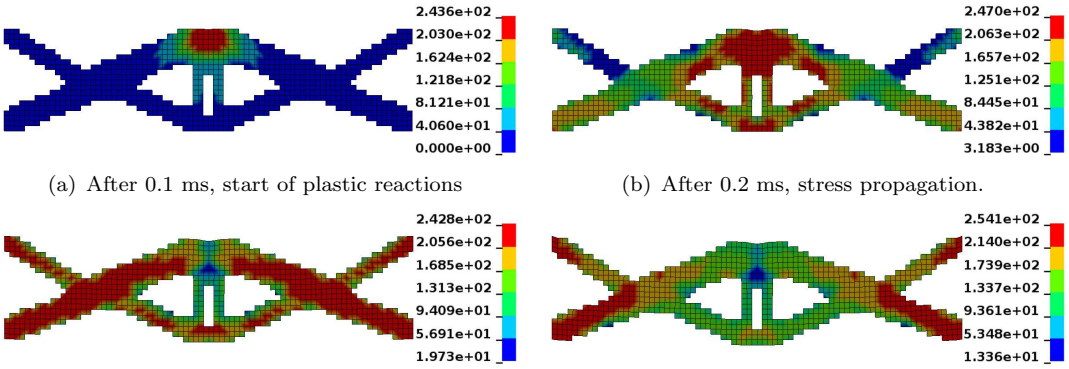

(a) After 0.1 ms, start of plastic reactions

(b) After 0.2 ms, stress propagation.

(c) After 0.4 ms, stress propagation.

(d) After 0.9 ms, time of maximal intrusion.

Figure 26. Von Mises stress distribution (in [MPa]) during the crash for the best design optimised for the impact velocity of 40 [m/s], for constant impact energy.

For the case of the highest impact velocity (and the lowest momentum), very high peak force in the initial phase of crash can be observed. At that point, most of the kinetic energy of the impactor is absorbed by plastification of the part of the structure being in a direct contact with the pole. Since the momentum of the impactor is very low, the pole is stopped after a very short time, according to the Newton's second law of motion. Thus, the mechanical behaviour of the topology optimised for high impact velocity is considerably different from the one optimised for low impact velocity, where the energy is absorbed much more uniformly by the whole structure.

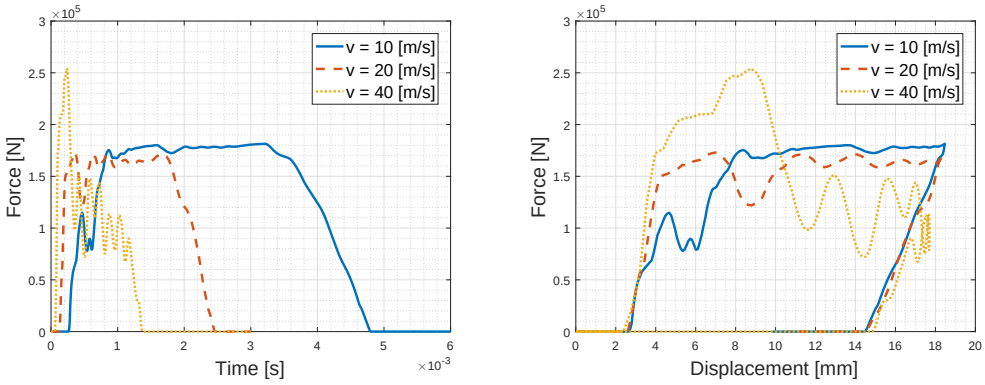

Figure 27. Evolution of the force acting on the impactor over time (left) and force-displacement curves (right) for the best designs for constant impact energy, optimised for different impact velocities.

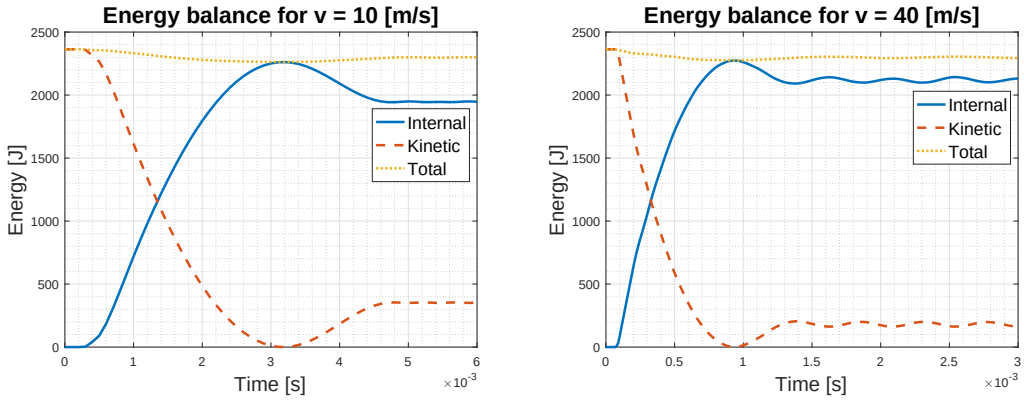

Figure 28. Energy balance for the best designs for constant impact energy, optimised for different impact velocities. Plot for 20 [m/s] the same as in Figure 22.

5.1.3. Influence of the mesh resolution

As in the case of the statically-loaded structure, an analysis of the influence of the finite element mesh resolution on the final topology, for the case of constant impactor mass, was carried out. This additional test was performed due to the non-linear character of crash simulations, which might make the dynamic case significantly different from the static one. In order to check if the mesh resolution might have an impact on the type of the obtained topology, 15 optimisation trials for a mesh resolution doubled in each direction, resulting in 8 times larger number of finite elements, were carried out. The best designs obtained for meshes consisting of 1600 and 12800 finite elements are compared in Table 8.

It seems that as in the static case, mesh resolution does not have a significant influence on the type of obtained topology, justifying the use of coarser meshes in favour of a more computationally efficient investigation of the optimisation method.

5.2. *Mass minimisation with intrusion and acceleration constraint*

In the context of crash optimisation of structures like side sills, which inspired the test cases considered in this work, it is important not only to reduce the intrusion of the impactor into the structure, but also to keep the maximal acceleration on an acceptable low level. This is dictated mainly by biomechanical injury criteria, like head

Table 8. Analysis of the influence of mesh resolution on the crash structures. The best designs obtained in 30 and 15 optimisation runs with coarse and fine FE mesh, respectively. Test case with constant impactor mass.

	Best designs for different mesh sizes	
Impact velocity	Mesh size: 80 x 20 x 1	Mesh size: 160 x 40 x 2
10 [m/s]		
20 [m/s]		
40 [m/s]		

injury criterion (HIC). The main objective of lightweight structural design is weight reduction, therefore, from engineering perspective, it is reasonable to consider a mass minimisation problem with constraints on intrusion and maximal acceleration. In this section, the results of crash TO of this test case, for impact velocity of 20 [m/s] and different values of maximal intrusions and accelerations, are presented.

5.2.1. Results

In Table 9, the best designs out of 30 optimisation trials for intrusion constraints of 15 [mm], 20 [mm], 25 [mm] and 30 [mm], are shown. In the ideal case, in order to minimise the maximal acceleration for a given crash duration, the acceleration should be constant during the whole crash event, until the impactor is stopped. Since this might be very challenging for the optimiser and not feasible in general case, we always choose the acceleration constraint on a level of 10% higher than the constant one, calculated according to the following formula:

$$a_{max} = \frac{v_0^2}{2d}, \tag{10}$$

where v_0 is the initial velocity and d is the intrusion of the impactor into the structure.

Performance of the optimised designs in terms of intrusions and accelerations are shown in Figure 29. The deformed structures and effective plastic strain distributions are presented in Figure 30. Force-displacement curves for the best designs are presented in Figure 31 and energy balance for those designs is shown in Figure 32.

The optimised topologies show an obvious tendency towards lower masses as the higher intrusions are allowed. It can be noted that the mass of the structure is approximately inversely proportional to the intrusion. A gradual transition from the hanging to supporting structure can be observed, as well. Interestingly, the best design for 15 [mm] intrusion constraint corresponds to the third best design in Table 5, emphasizing the fact that the search for different optima might be beneficial in the engineering

Table 9. Comparison of the best designs for mass minimisation problem with intrusion and acceleration constraint.

Design	Characteristics of the design		
	Intrusion	Maximal deceleration	Mass
	15 [mm]	$1.4239 \cdot 10^7$ [mm/s^2]	2.214 [kg]
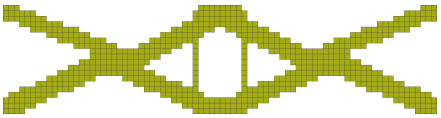	20 [mm]	$1.0566 \cdot 10^7$ [mm/s^2]	1.647 [kg]
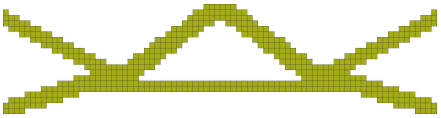	25 [mm]	$8.6117 \cdot 10^6$ [mm/s^2]	1.312 [kg]
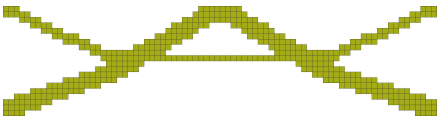	30 [mm]	$7.3057 \cdot 10^6$ [mm/s^2]	1.110 [kg]

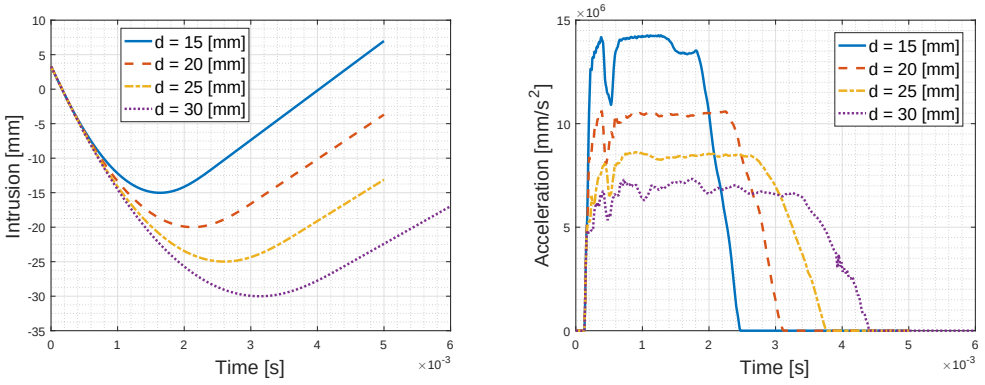

Figure 29. Intrusions and accelerations for the best designs for mass minimisation problem with intrusion and acceleration constraint.

practice, when the inferior optimum may become the best option as soon as some of the initially neglected constraints are taken into account.

As can be seen in Figure 30, for higher intrusions, the algorithm tends to develop structures exhibiting two-phase crash behaviour, allowing for further reduction of the maximal acceleration of the impactor. For example, the structure optimised for 25 [mm] intrusion constraint, in the first phase of the crash (corresponding to ca. 1.5 [ms]), deforms similarly to the structures obtained for the intrusion minimisation case. However, in the second phase, the upper part of the structure, consisting of two beams being in contact with the impactor, is strongly compressed, absorbing most of the remaining kinetic energy of the pole. In case of the design optimised for 30 [mm]

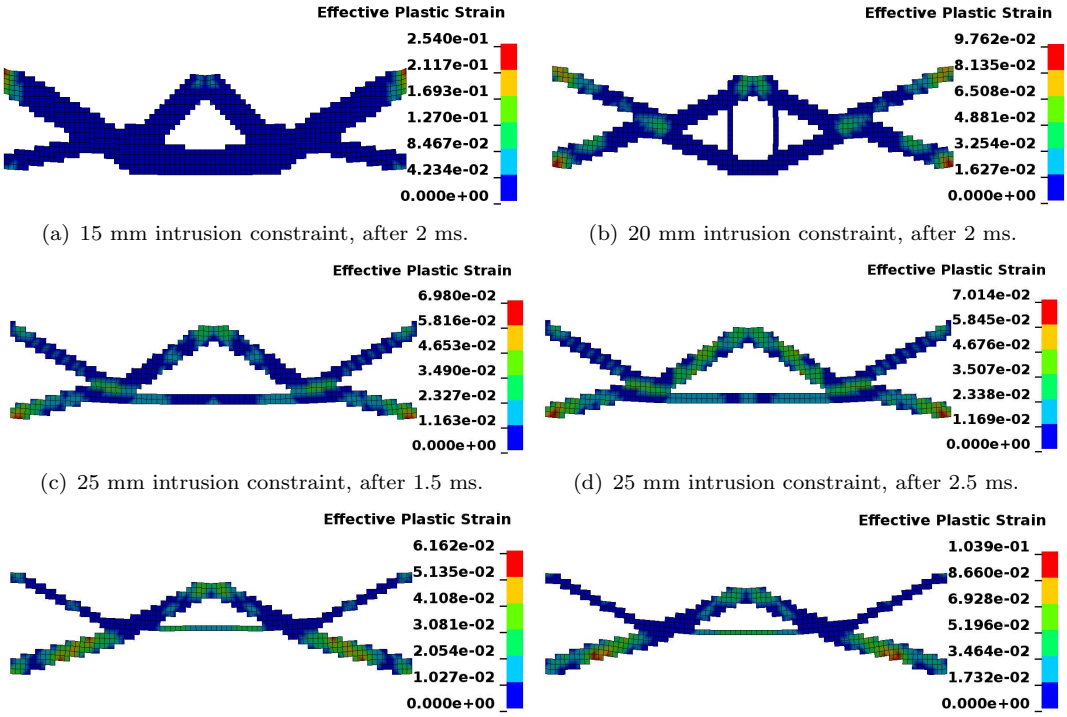

(a) 15 mm intrusion constraint, after 2 ms.

(b) 20 mm intrusion constraint, after 2 ms.

(c) 25 mm intrusion constraint, after 1.5 ms.

(d) 25 mm intrusion constraint, after 2.5 ms.

(e) 30 mm intrusion constraint, after 1.5 ms.

(f) 30 mm intrusion constraint, after 3.5 ms.

Figure 30. Deformed structures and effective plastic strain distribution for the best designs for mass minimisation problem with intrusion and acceleration constraint.

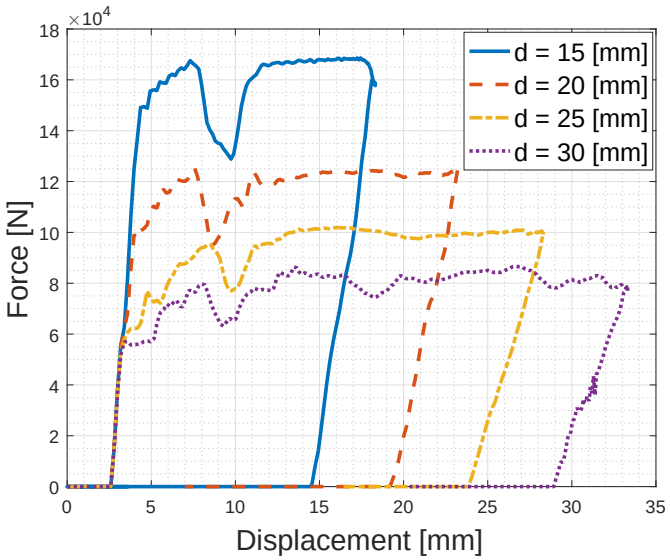

Figure 31. Force-displacement curves for the best designs for mass minimisation problem with intrusion and acceleration constraint.

intrusion constraint, again, a typical behaviour of the structures optimised for minimal intrusion can be observed in the first phase of the crash. However, after ca. 1.5 [ms], the beams in the bottom corners of the design domain start to buckle. Most probably, the tendency towards the buckling behaviour and the further mass reduction would be kept as higher intrusions are allowed. For those cases, the buckling behaviour can no

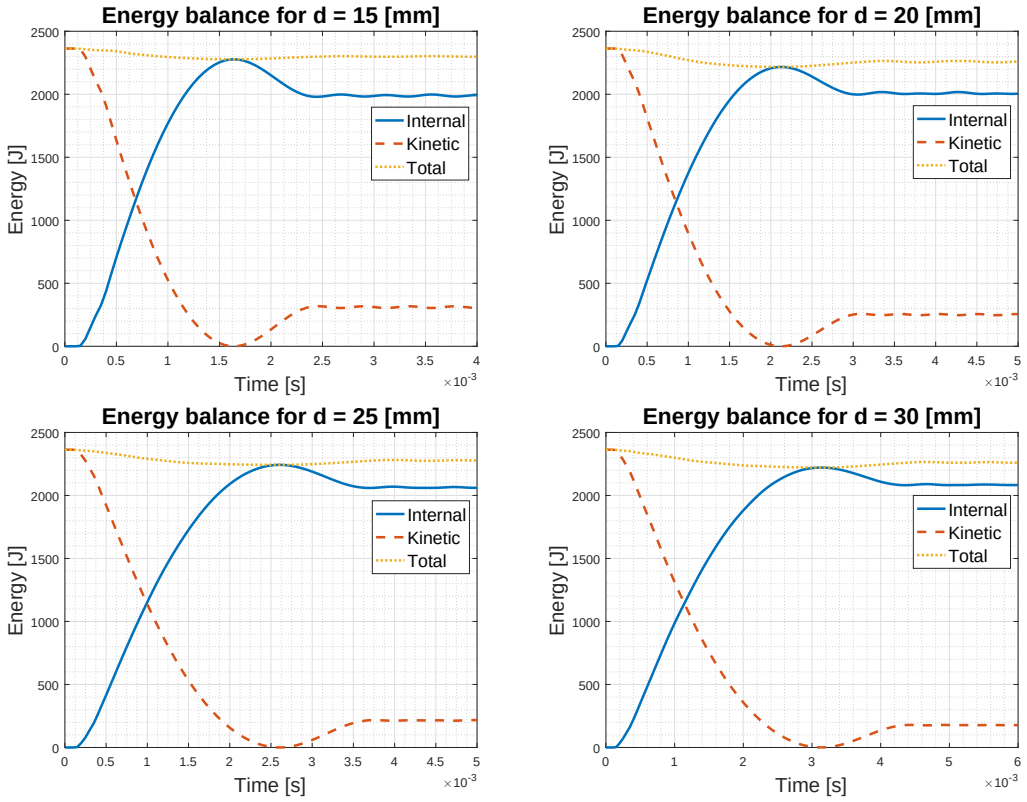

Figure 32. Energy balance for the best designs for mass minimisation problem with intrusion and acceleration constraint.

longer be simulated properly with reasonably low number of finite elements (especially in the context of optimisation). Preferably, the investigations concerning optimal crash structures should be continued with a different approach, based on shell finite elements, like the evolutionary crash topology optimisation method for thin-walled structures [12].

6. Summary

In this paper, a novel, evolutionary level set method (EA-LSM) [13] was used for investigations regarding optimal topologies of crash structures. The method benefits from an implicit parametrisation of structural design by a set of level set basis functions, which allows for a significant reduction of the number of design variables and an efficient optimisation with non-gradient methods. Unlike in the state-of-the-art methods for crash topology optimisation, no heuristic assumptions have to be used, which, together with the superior global search properties of evolutionary algorithms, gives the possibility to obtain a reliable information about the optima of crash problems. The method is validated on a linear elastic test case by comparison with the SIMP approach.

The experimental part of the paper is devoted to identification of the best designs for a two-dimensional, transverse bending crash case. Here, two different optimisation problems were considered: intrusion minimisation with mass constraint and mass minimisation with intrusion and acceleration constraint. The results show a dependency

between impact velocity and the type of obtained topologies both when mass of the impactor and impact energy are kept constant. It turns out that the designs obtained for intermediate velocity levels exhibit more similarities to the topologies optimised for the static case than the ones optimised for very low impact velocities. This questions the frequent assumption that the optimisation of a static replacement load will lead to optimal structures for the actual crash load, as used in equivalent static loads (ESL) methods. Furthermore, a high concentration of internal energy in selected parts of the structure for both optimisation cases and a relatively good homogeneity of equivalent stress distribution for the intrusion minimisation case were observed. For these cases, the energy absorption homogenisation criterion used in the hybrid cellular automata (HCA) techniques seems to be not really valid and a design rule closer to the idea of the fully stressed design should be considered.

Convergence velocity of the method is determined by the cost of evolution strategies, which rises with the number of design variables. This, however, can be mitigated with parallelisation of computations, which can be done very efficiently for evolutionary algorithms and the computational costs could be further reduced with hybridisation techniques [14]. With use of these techniques, application of the method to three-dimensional cases seems to be straightforward and very promising. EA-LSM offers great flexibility, allowing for incorporation of different objectives and constraints. Thanks to generality of the method, more complex material models, accounting for strain rate effects or failure, can be easily used. Finally, universality of evolutionary algorithms makes the approach applicable to a wide range of structural topology optimisation problems in many industrial applications.

References

[1] G. Allaire, E. Bonnetier, G. Francfort, and F. Jouve, *Shape optimization by the homogenization method,* Numer. Math., 76 (1997), pp. 27–68.

[2] G. Allaire, F. Jouve, and A.-M. Toader, *Structural optimization using sensitivity analysis and a level-set method,* J. Comput. Phys., 194 (2004), pp. 363–393.

[3] G. Allaire, F. De Gournay, F. Jouve, and A. Toader, *Structural optimization using topological and shape sensitivity via a level set method, Control Cybernet.* 34 (2005), pp. 59–80.

[4] N. Aulig, S. Menzel, E. Nutwell and D. Detwiler, *Towards multi-objective topology optimization of structures subject to crash and static load cases,* 4th International Conference on Engineering Optimization, Lisbon, Portugal, 2014.

[5] N. Aulig, S. Menzel, E. Nutwell and D. Detwiler, *Preference-based topology optimization of body-in-white structures for crash and static loads,* 14th LS-DYNA International Conference, Dearborn, MI, USA, 2016.

[6] N. Aulig, and M. Olhofer, *State-based representation for structural topology optimization and application to crashworthiness,* IEEE Congress on Evolutionary Computation, Vancouver, Canada, 2016.

[7] M. P. Bendsøe, *Optimal shape design as a material distribution problem,* Struct. Optim. 1 (1989), pp. 193–202.

[8] M. P. Bendsøe and N. Kikuchi, *Generating optimal topologies in structural design using a homogenization method,* Comput. Methods Appl. Mech. Engrg. 71 (1988), pp. 197–224.

[9] M. P. Bendsøe and O. Sigmund, *Topology Optimization*, Springer Berlin Heidelberg, Germany, 2004.

[10] T. Buhl, C. B. W. Pedersen, and O. Sigmund, *Stiffness design of geometrically nonlinear structures using topology optimization,* Struct. Multidisc. Optim. 19 (2000), pp. 93–104.

[11] M. Bujny, *Development of a hybrid evolutionary approach for level set topology optimization*, MSc thesis, Technical University of Munich, Germany, 2015.

[12] M. Bujny, N. Aulig, M. Olhofer, and F. Duddeck, *Evolutionary crashworthiness topology optimization of thin-walled structures,* 11th ASMO UK / ISSMO / NOED2016: International Conference on Numerical Optimisation Methods for Engineering Design, Munich, Germany, 2016.

[13] M. Bujny, N. Aulig, M. Olhofer, and F. Duddeck, *Evolutionary level set method for crashworthiness topology optimization,* ECCOMAS Congress 2016, Crete Island, Greece, 2016.

[14] M. Bujny, N. Aulig, M. Olhofer, and F. Duddeck, *Hybrid evolutionary approach for level set topology optimization,* IEEE Congress on Evolutionary Computation, Vancouver, Canada, 2016.

[15] M. Cavazzuti, A. Baldini, E. Bertocchi, D. Costi, E. Torricelli, and P. Moruzzi, *High performance automotive chassis design: a topology optimization based approach,* Struct. Multidisc. Optim. 44 (2010), pp. 45–56.

[16] J. Christensen, C. Bastien, and M. V. Blundell, *Effects of roof crush loading scenario upon body in white using topology optimisation,* Int. J. Crashworthiness 17 (2012), pp. 29–38.

[17] C. A. Coello Coello, *Theoretical and numerical constraint-handling techniques used with evolutionary algorithms: a survey of the state of the art,* Comput. Methods Appl. Mech. Engrg. 191 (2002), pp. 1245–1287.

[18] N. P. v. Dijk, K. Maute, M. Langelaar, and F. v. Keulen, *Level-set methods for structural topology optimization: a review,* Struct. Multidisc. Optim. 48 (2013), pp. 437–472.

[19] F. Duddeck, S. Hunkeler, P. Lozano, E. Wehrle, and D. Zeng, *Topology optimization for crashworthiness of thin-walled structures under axial impact using hybrid cellular automata,* Struct. Multidisc. Optim. 54 (2016), pp. 415-428.

[20] F. Duddeck and K. Volz, *A new topology optimization approach for crashworthiness of passenger vehicles based on physically defined equivalent static loads,* ICRASH Conference, Milano, Italy, 2012.

[21] H. Fredricson, T. Johansen, A. Klarbring, and J. Petersson, *Topology optimization of frame structures with flexible joints,* Struct. Multidisc. Optim. 25 (2003), pp. 199–214.

[22] X. Guo, W. Zhang and W. Zhong, *Doing topology optimization explicitly and geometrically - a new moving morphable components based framework,* J. Appl. Mech. 81 (2014), pp. 31–32.

[23] N. Hansen and A. Ostermeier, *Adapting arbitrary normal mutation distributions in evolution strategies: the covariance matrix adaptation,* Proceedings of IEEE International Conference on Evolutionary Computation, pp. 312–317, 1996.

[24] K. Hamza, M. Aly and H. Hegazi, *A kriging-interpolated level-set approach for structural topology optimization,* J. Mech. Design 136 (2014), pp. 011008–011008–12.

[25] N. Hansen and A. Ostermeier, *Completely derandomized self-adaptation in evolution strategies,* Evol. Comput. 9 (2001), pp. 159–195.

[26] N. Hansen, *The CMA Evolution Strategy: A Comparing Review,* in *Studies in Fuzziness and Soft Computing 192*, J. A. Lozano, P. Larrañaga, I. Inza, and E. Bengoetxea, eds., Springer Berlin Heidelberg, Germany, 2006, pp. 75–102.

[27] N. Hansen and S. Kern, *Evaluating the CMA evolution strategy on multimodal test functions,* in *Lecture Notes in Computer Science 3242,* X. Yao, E. K. Burke, J. A. Lozano, J. Smith, J. J. Merelo-Guervós, J. A. Bullinaria, J. E. Rowe, P. Tiňo, A. Kabán, and H.-P. Schwefel, eds., Springer Berlin Heidelberg, Germany, 2004, pp. 282–291.

[28] N. Hansen, S. Müller, and P. Koumoutsakos, *Reducing the time complexity of the derandomized evolution strategy with covariance matrix adaptation (CMA-ES),* Evol. Comput. 11 (2003), pp. 1–18.

[29] B. Hassani and E. Hinton, *A review of homogenization and topology optimization homogenization theory for media with periodic structure,* Comput. Struct. 69 (1998), pp. 707–717.

[30] S. Hunkeler, *Topology optimisation in crashworthiness design via hybrid cellular automata for thin-walled structures*, Ph.D. diss., Queen Mary University of London, UK, 2013.
[31] C. K. Mozumder, *Topometry optimization of sheet metal structures for crashworthiness design using hybrid cellular automata*, Ph.D. diss., University of Notre Dame, USA, 2010.
[32] S. D. Müller, N. Hansen, and P. Koumoutsakos, *Increasing the serial and the parallel performance of the CMA-evolution strategy with large populations,* in *Lecture Notes in Computer Science 2439*, J. J. M. Guervós, P. Adamidis, H.-G. Beyer, H.-P. Schwefel, and J.-L. Fernández-Villacañas, eds., Springer Berlin Heidelberg, Germany, 2002, pp. 422–431.
[33] C. Ortmann and A. Schumacher, *Graph and heuristic based topology optimization of crash loaded structures,* Struct. Multidisc. Optim., 47 (2013), pp. 839–854.
[34] S. Osher and R. P. Fedkiw, *Level set methods: an overview and some recent results,* J. of Comput. Phys., 169 (2001), pp. 463–502.
[35] G.-J. Park, *Technical overview of the equivalent static loads method for non-linear static response structural optimization,* Struct. Multidisc. Optim. 43 (2010), pp. 319–337.
[36] N. M. Patel, *Crashworthiness design using topology optimization,* Ph.D. diss., University of Notre Dame, USA, 2007.
[37] C. B. W. Pedersen, *Topology optimization design of crushed 2d-frames for desired energy absorption history,* Struct. Multidisc. Optim. 25 (2003), pp. 368–382.
[38] S. S. Rao, *Engineering Optimization: Theory and Practice*, John Wiley & Sons, 2009.
[39] G. I. N. Rozvany, M. Zhou, and T. Birker, *Generalized shape optimization without homogenization,* Struct. Optim. 4 (1992), pp. 250–252.
[40] J. A. Sethian, *Evolution, implementation, and application of level set and fast marching methods for advancing fronts,* J. Comput. Phys., 169 (2001), pp. 503–555.
[41] O. Sigmund, *A 99 line topology optimization code written in Matlab,* Struct. Multidisc. Optim. 21 (2014), pp. 120–127.
[42] K. Suzuki and N. Kikuchi, *A homogenization method for shape and topology optimization,* Comput. Methods Appl. Mech. Engrg. 93 (1991), pp. 291–318.
[43] M. Y. Wang, X. Wang, and D. Guo, *A level set method for structural topology optimization,* Comput. Methods Appl. Mech. Engrg. 192 (2003), pp. 227–246.
[44] M. Yulin and W. Xiaoming, *A level set method for structural topology optimization and its applications,* Adv. Engrg. Softw. 35 (2004), pp. 415–441.
[45] D. Zeng and F. Duddeck, *Improved hybrid cellular automata for crashworthiness optimization of thin-walled structures,* Struct. Multidisc. Optim. (2017).